Available online at www.sciencedirect.com

ScienceDirect

Procedia CIRP 94 (2020) 722–725

www.elsevier.com/locate/procedia

11th CIRP Conference on Photonic Technologies [LANE 2020] on September 7-10, 2020

Numerical study of additional element transport in wire feed laser beam welding

Xiangmeng Meng[a,*], Antoni Artinov[a], Marcel Bachmann[a], Michael Rethmeier[b,a]

a BAM Federal Institute for Materials Research and Testing, Unter den Eichen 87, 12205 Berlin, Germany

b Technical University Berlin, Institute of Machine Tools and Factory Management, Pascalstraße 8-9, 10587 Berlin, Germany

* Corresponding author. Tel.: +49 30 8104 4788; *E-mail address:* Xiangmeng.Meng@bam.de

Abstract

The transport phenomena in the wire feed laser beam welding are investigated numerically. A three-dimensional transient heat transfer and fluid flow model coupled with free surface tracing and element transport is developed. A ray-tracing method with local grid refinement algorithm is used to calculate the multiple reflections and Fresnel absorption on the keyhole wall. The filler material flows backward along the lateral side of the weld pool, and subsequently flows forward along the longitudinal plane. The occurrence of the bulging phenomenon may further prevent the downward transfer of the additional elements to the root of the weld pool.

Keywords: Laser beam welding; Element tranport; Filler wire; Numerical modelling

1. Introduction

As the rapid development of different types of laser sources, the laser beam with high power density and good beam quality is easily accessed, which makes deep penetration laser beam welding (LBW) become one of the most widely used and promising joining techniques in modern industry [1]. Some issues, however, may be encountered during the application of the autogenous LBW. Firstly, the small size of the laser spot requires strict assembly tolerance. Secondly, the extremely high energy density of the laser beam may cause loss of the alloying element due to severe metal evaporation.

The aforementioned issues can be solved by introducing additional filler wire to the autogenous LBW, namely wire feed laser beam welding (WFLBW). The melted filler material can improve the capacity of gap bridging. Furthermore, some desirable alloying elements can be added into the weld pool, controlling the metallurgical behavior and improving the weld properties eventually [2]. However, a uniform distribution of the filler material can hardly be achieved due to the high cooling rate of the weld pool. A strong gradient of the additional element was observed along the vertical direction [3]. Although some methods have been proposed to enhance the material mixing in the WFLBW such as hot wire technique [4], laser oscillation technique [5] and electromagnetic stirring technique [6], the quantitative characterization of the element transport is still very rare.

The objective of the present study is to visualize the dynamic element transport in the weld pool of the WFLBW using a 3D transient computational fluid dynamic (CFD) model. A ray-tracing method with local grid refinement algorithm is implemented to calculate the multiple reflections and Fresnel absorption on the keyhole wall. The temperature distribution, velocity field, dynamic keyhole profile and the element transfer are calculated numerically. The model is verified by experimental results. The work can provide a quantitative explanation for the occurrence of the inhomogeneity of the additional material in WFLBW. It may also give some

10.1016/j.procir.2020.09.129

inspirations for the technical improvement to enhance the material mixing during WFLBW.

2. Mathematical formula

Necessary simplifications are made to capture the key features of the WFLBW meanwhile reduce the computational intensity.

- The density is considered as a constant value, and the Boussinesq approximation is used for the buoyancy term.
- The flow is laminar and Newtonian.
- The melting of the filler wire under laser irradiation is not simulated. Instead, a mass inlet with appropriate temperature and velocity is set for the transfer of the liquid filler metal.

During deep penetration LBW, the most important physics occurred are the multiple reflections of the laser beam on the keyhole wall and the Fresnel absorption at each reflection point. A ray tracing method is usually used to describe the spatial distribution of laser energy on the keyhole wall, in which the laser beam is discretized into thousands of sub-rays with location-dependent energy densities and initial incidence angles [7]. However, the radius of the laser spot is almost comparable with the commonly used cell size in the numerical model (0.05 mm ~ 0.2 mm), which is a strong limitation for the accuracy of the ray tracing method, as shown in Fig. 1a.

In this study, the basic ray tracing method is improved by a local grid refinement algorithm. Firstly, the basic ray tracing method is applied to search the potential reflection cell. According to the volume fraction of metal (F) and the normal vector of the free surface $\vec{N} = \nabla F$ in this cell, the distance between the free surface and the cell center can be calculated by the piecewise linear interface calculation (PLIC) method [8]. Therefore, by taking the cell center as the origin, the mathematical equation of the free surface can be written as:

$$n_x x + n_y y + n_z z = D \quad (1)$$

where D is Distance from free surface to cell center, n_x, n_y, and n_z are x,y,z components of normal vector.

Then the reflection cell is refined locally by the virtual sub-cells, as shown in Fig.1b. The sub-cells which are located on the free surface can be easily identified by Eq. (1), as colored as green in Fig. 1b. Therefore, a more accurate reflection point can be determined among these sub-cells without refining the real geometry mesh in the model.

The governing equations including mass equation, momentum equation, volume-of-fluid (VOF) equation and element transport equation are solved by the commercial software ANSYS Fluent 19.3 to get the temperature and velocity fields, free surface deformation and element distribution.

The energy balance between the laser energy, the thermal conduction into the metal and the thermal dissipation (convection, radiation and evaporation) are calculated. The keyhole profile is determined by the dynamic balance between recoil pressure, Laplace pressure, hydrostatic pressure and hydrodynamic pressure. The temperature and velocity of the melting filler material are taken from literature [9,10]. The latent heat release from the metal vapor's re-condensation and the additional heating effect from the high-temperature plume are considered [11]. The momentum impact from the high-speed metal vapor is also applied by an empirical model [7].

The mathematical descriptions of the numerical model can be found in detail in the authors' previous works [12,13].

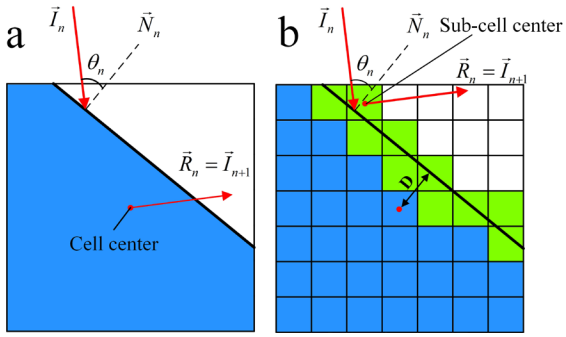

Fig. 1. The schematic of ray tracing method: (a) based on original cell size, (b) with local grid refinement algorithm

3. Experimental methods

An austenitic stainless steel (AISI 304) was chosen as the base metal. A nickel-based filler wire (Inconel 625) was used. The dimension of the base metal was 200 mm × 60 mm × 10 mm, and the filler wire had a diameter of 1.2 mm. A significant difference of Ni content exists between the base metal and the filler wire (8.7 % vs. 58.0 %), so the Ni can be used as a marking element to describe the material mixing in the molten pool.

The welding was performed by an IPG YLR 20000 fiber laser system. Butt configuration was carried out with technical zero gap. The wire was fed with a leading position and had 57° angle with respect to the optical axis of the laser. The pure Argon shielding gas was provided behind the laser spot. The welding parameters used are listed in Table 1.

Table 1. Welding parameters and laser properties

Laser power	7.5 kW
Laser spot diameter	0.52 mm
Fiber diameter	0.2 mm
Collimation length	125 mm
Wavelength	1070 nm
Focal length	350 mm
Focal position	-3 mm
Welding speed	1.3 m/min
Wire feeding speed	2.1 m/min
Shielding gas	20 l/min

Optical microscopy observation was performed on the transverse section to reveal the fusion zone shape. The energy dispersive X-ray spectroscopy (EDX) mapping was conducted to measure the Ni content on the transverse section.

4. Results and discussion

Fig. 2 gives the comparison between the calculated fusion line and the experimental one. Not only the fusion line but also the reinforcement profile is predicted accurately, which proves the physical reasonability of the current model. The experimental weld is not perfectly symmetric with respect to the joining interface due to the assembly tolerance.

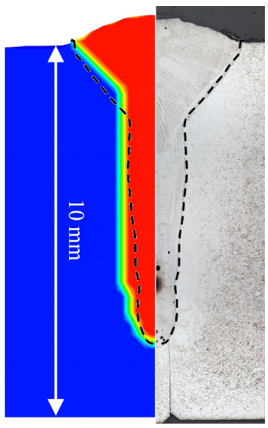

Fig. 2. Comparison between calculated and experimental fusion lines (red: weld zone, blue: unmelted metal, green: semi-melted fusion line).

The 3D temperature distribution and velocity field at the longitudinal section and the top free surface are shown in Fig. 3. The black line shows the liquidus temperature. The weld pool is elongated at the top region to form a typical teardrop shape. A bulging region is observed at the bottom region of the weld pool. The bulging phenomena have also been found in other experimental and numerical studies and may contribute to the formation of some defects such as hot cracking [11,14]. The weld pool becomes relatively narrow between the top region and the bulging region.

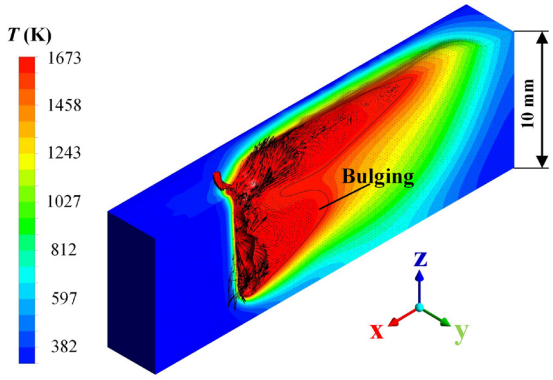

Fig. 3. 3D Temperature distribution and velocity field

At the top region, the liquid metal flows backward along the weld pool surface and then forward along the longitudinal section. At the bulging region, the liquid metal flows backward along the boundary of the weld and its flowing direction changes later to become forward. These two dominant circulations are almost separated by the narrowed region. It implies that the formation of the bulging may show significant influence on the basic flow pattern of the weld pool.

The transport of the filler material is directly determined by the thermo-fluid flow. Fig. 4 shows the Ni transport in the weld pool. The liquid filler material with higher Ni content first impacts on the keyhole front wall. Subsequently, the filler material flows backward along the lateral side of the weld pool. As the flowing direction of the top circulation changes from backward to forward, the added Ni element is brought to the forepart of the weld pool. This vigorous top circulation produces a homogeneous Ni distribution at the top region.

Since the weld pool is significantly narrowed between the top region and the bulging region, the downward channel is blocked. The additional Ni cannot be transferred from the top region to the root of the weld pool. Our preliminary works suggest that the bulging phenomena give detrimental influence on the mixing of the filler material. Further experimental verifications are still needed, and more analyses should be performed on its formation mechanism in the future.

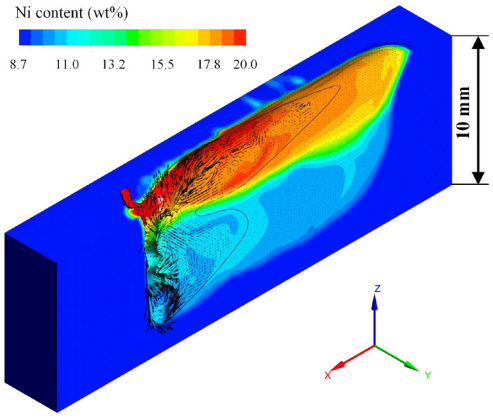

Fig. 4. 3D transport route of Ni element

Fig. 5a shows the calculated Ni distribution on the cross-section of the final weld. The additional Ni concentrates on the upper part of the weld. The well-mixed depth is only 3.2 mm which is 40 % of the penetration depth. By comparing the EDX mapping in Fig. 5b, a good agreement between numerical and experimental results is confirmed again.

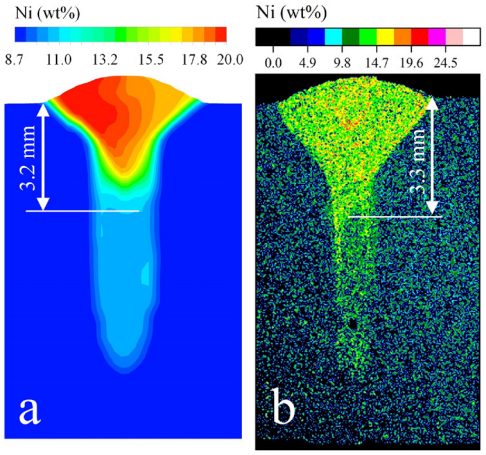

Fig. 5. Ni distribution on cross-section of final weld: (a) numerical result, (b) EDX mapping

5. Conclusions

(1) A 3D transient CFD model is developed to investigate the additional element transport in the wire feed laser beam welding. A local grid refinement algorithm is developed to improve the accuracy of the ray tracing method.

(2) A bulging region is observed at the bottom of the weld pool. The weld pool is significantly narrowed between the top region and the bulging region.

(3) The additional filler material flows backward along the lateral side of the weld pool and then flows forward along the longitudinal section to bring the Ni to the forepart of weld pool. The occurrence of the bulging phenomenon may further prevent the downward transfer of the additional elements to the root of the weld pool.

Acknowledgements

This work is funded by the Deutsche Forschungsgemeinschaft (DFG, German Research Foundation) – project Nr. 416014189 (BA 5555/6-1) and Nr. 411393804 (BA 5555/5-1).

References

[1] Bachmann M, Gumenyuk A, Rethmeier M. Welding with high-power lasers: trends and developments, Phys. Procedia 2016;83:15–25.
[2] Zhang K, Li D, Gui H, Li Z. Adaptive control for laser welding with filler wire of marine high strength steel with tight butt joints for large structures. J Manuf Process 2018;36:434-41.
[3] Seefeld T, Buschenhenke F, Vollertsen F. Laser beam welding with hypereutectic AlSi filler material. In International Congress on Applications of Lasers & Electro-Optics 2009.
[4] Wang L, Gao M, Hao Z. A pathway to mitigate macrosegregation of laser-arc hybrid Al-Si welds through beam oscillation. Int J Heat Mass Transf 2020;151:119467.
[5] Zheng S, Wen P, Shan J. Experimental analysis on fusion ratio and composition uniformity of laser hot wire welds. Trans China Weld Inst, 2012;33:45-48.
[6] Gatzen M. Influence of low-frequency magnetic fields during laser beam welding of aluminium with filler wire. Phys Procedia 2012;39:59–66.
[7] Cho WI, Na SJ, Thomy C, Vollertsen F. Numerical simulation of molten pool dynamics in high power disk laser welding. J Mater Process Technol 2012;212:262–75.
[8] Youngs DL. An interface tracking method for a 3D Eulerian hydrodynamics code. Atomic Weapons Research Establishment (AWRE) Technical Report 1984; 44: 35.
[9] Arata Y, Maruo H, Miyamoto I, Nishio R. High power CO_2 laser welding of thick plate: multipass weding with filler wire (welding physics, process & instrument). Trans JWRI 1986;15:199-206.
[10] Salminen A. The filler wire–laser beam interaction during laser welding with low alloyed steel filler wire. Mechanika 2010;4:67–75.
[11] Muhammad S, Han SW, Na SJ, Gumenyuk A, Rethmeier M. Study on the role of recondensation flux in high power laser welding by computational fluid dynamics simulations. J Laser Appl 2018;30:012013.
[12] Meng X, Bachmann M, Artinov A, Rethmeier M. Experimental and numerical assessment of weld pool behavior and final microstructure in wire feed laser beam welding with electromagnetic stirring. J Manuf Process 2019;45:408-418.
[13] Meng X, Artinov A, Bachmann M, Rethmeier M. Numerical and experimental investigation of thermo-fluid flow and element transport in electromagnetic stirring enhanced wire feed laser beam welding. Int J Heat Mass Transf 2020;144:118663.
[14] Artinov A, Bakir N, Bachmann M, Gumenyuk A, Rethmeier M. Weld pool shape observation in high power laser beam welding. Procedia CIRP 2018;74:683-686.